Chirp evaluation of 850 nm single mode VCSEL exploiting modal noise in standard single mode fiber

Jacopo Nanni, Jean-Luc Polleux, Catherine Algani,
Simone Rusticelli, Federico Perini, Giovanni Tartarini *Member, IEEE,*

***Abstract*—The phenomenon of modal noise, which is typically undesired within fiber optic links, is exploited advantageously to characterize Vertical Cavity Surface Emitting Lasers (VCSELs) operating in the first optical window (wavelength $\lambda \simeq 850nm$), in terms of frequency chirping.**

The proposed method, which can be applied utilizing ordinary laboratory components and instrumentation, contributes to fill an existing gap. Indeed, the methods which are typically exploited to determine this undesired optical frequency modulation can be straightforwardly applied only to sources operating at wavelengths of 1310 nm and 1550 nm, while they become unpractical or even inapplicable at wavelengths of 850 nm.

Through the proposed technique, the evaluation of the VCSEL chirping parameters can be performed, which allows the correct design of various types of fiber optic links making possible to take advantage of these low-cost and low-consumption optical sources.

***Index Terms*—Surface-emitting lasers; Measurement; Chirp modulation; Optical fiber communication.**

I. Introduction

Vertical Cavity Surface Emitting Lasers (VCSELs) operating in the first optical window (wavelength $\lambda \simeq 850nm$) are very attractive optical sources, due to their low cost and reduced level of power consumption, and can be utilized either for the transmission of digital [1], [2] or Radio Frequency (RF) [3] signals.

Since a direct modulation of the optical carrier is typically performed on VCSELs, the correct design of the relevant link requires the knowledge of their performances in terms of frequency chirp. Indeed, directly modulated semiconductor lasers exhibit this generally undesired phenomenon, which is due to the change of refractive index with the modulating signal [4]–[6].

For fiber links of the order of some kilometers or tens of kilometers, which usually operate in single mode regime, laser frequency chirp, combined with fiber chromatic dispersion, can generate at the receiver side undesired spurious frequencies terms [7] and/or the increase of quantities like the Adjacent Channel Leakage Ratio (ACLR) [8] or the Bit Error Rate [9].

Also for short range links, which often operate in multimode regime, the chirp phenomenon can cause impairments in the quality of the received signal. Indeed, in this case, it increases the impact of modal noise [10], which results in fluctuations of the output signal level [11] and increase of distortion terms [12] when the fiber is subjected to temperature variations or mechanical stress, and can produce a temporary out of service of the link.

The latter framework is the one in which fiber links utilizing $\lambda \simeq 850nm$ VCSELs typically operate. Indeed, the levels of optical power and fiber attenuation do not allow to cover high distances. At the same time a multimodal behavior takes place when the optical channel is constituted not only by Multimode Fibers (MMFs), e.g. with standard core diameters of 50 μm or 62.5 μm, but also by fibers with core diameter of about 9 μm, like the ones complying to ITU-T G652 Recommendation, which also allow more than one optical mode to propagate if operated in the first optical window [13].

Both mentioned configurations can be found in in the context of next generation Home Area Networks (HANs) where the VCSEL has been included among the possible optical transmitters in new mm-wave standard Wi-Fi 802.11ad [3] or in Passive Optical Networks (PON) to reduce costs and consumption [14]. Moreover, they have potential applications in the field of Radioastronomy [15] where a high number of Radio-over-Fiber (RoF) links based on 850 nm VCSEL can be utilized to carry the RF signals received from the celestial radio sources to the processing facilities located at the antenna pedestal. Various methods have been proposed for measuring the chirp coefficient of laser sources [16]–[18]. In all cases, the setups utilized require to have single mode behavior of the optical link.

This allows to use the standard G.652 fiber, when a wavelength greater than about 1260 nm characterizes the emission of the considered laser [19], [20]. However, when sources emitting at 850 nm are considered, the application of these techniques becomes difficult.

Indeed, to operate in single mode regime at 850 nm it would be necessary to utilize relatively long spans of expensive non standard optical fibers exhibiting core diameters of a few micrometers. At the same time, problems related to low power levels at destination could arise, due to the generally not-high levels of optical power emitted by VCSELs, to the low coupling factor of the laser with short-core fibers, and to the relatively high attenuation exhibited by Silica at 850 nm. On

J. Nanni and G.Tartarini are with the Dipartimento di Ingegneria dell'Energia Elettrica e dell'Informazione "Guglielmo Marconi", Università di Bologna, 40136 Bologna, Italy (e-mail: jacopo.nanni3@unibo.it; giovanni.tartarini@unibo.it).

J.L.Polleux is with Université Paris-Est, ESYCOM (EA2552), ESIEE Paris, UPEM, Le Cnam, 93162 Noisy-le-Grand, France (e-mail: jean-luc.polleux@esiee.fr).

C.Algani is with Le Cnam, ESYCOM (EA2552), 75003 Paris, France (e-mail: catherine.algani@cnam.fr).

F.Perini and S.Rusticelli are with Institute of Radio Astronomy, National Institute for Astrophysics, Via Fiorentina 3513, 40059 Medicina, Italy (e-mail: f.perini@ira.inaf.it;rusticel@ira.inaf.it).

the other hand if one wants to utilize G.652 fiber span this is possible, but modal dispersion and fluctuations due to modal noise risk to let the measurements be much affected by error.

The method proposed in [21], based on a scanned optical filtering, can actually be applied also in reference to sources operating in the first optical window. The spurious phase deviation produced by frequency chirp is in this case determined through the evaluation of the linewidth enhancement factor α of the source considered. However, this determination is strictly rigorous only when the optical frequency deviation of the source is proportional to the derivative of the signal which modulates its emitted optical power. This type of frequency chirp is generally called *transient* and it is present for high frequency analog modulation or for high data rate digital transmissions.

However, a chirp characterization at lower frequency is also necessary for RoF-based applications such as in the Radioastronomic field [22] and in the HANs contexts cited above, in which signals are transmitted with a RF carrier below 1 GHz (e.g. LTE-A systems operating at 800 MHz) [23], [24]. This type of chirp is called *adiabatic*, since the frequency deviation is proportional to optical modulated signal. In this paper a novel measurement technique is proposed for the evaluation of the frequency chirp of single mode VCSELs which operate in the first optical window. This method represents a more general work of the Interferemotry-Based technique proposed in [25] for 1310 nm and 1550 nm DFB lasers, in which here both transient and adiabatic chirp are evaluated. The need of an optical interferometer is replaced by the exploitation of the multimodal propagation in standard single mode fiber.

The paper is organized as follows. Section II explains briefly the method proposed. Section III is dedicated to a detailed and complete mathematical description of the method proposed, proving the possibility of measuring the chirp coefficients exploiting modal noise. In Section IV the method is experimentally applied to a 850 nm Single Mode (SM) source and the chirp coefficients are evaluated showing the dependence on RF frequency of the intensity modulation and on the biasing current. The validation of the method is then performed employing the delayed self-homodyne technique proposed in [17] which is taken as reference. Finally conclusions will be drawn.

II. Proposed Method Description and Chirp Characterization System

The method proposed in this work is based on the dependence on frequency chirping, of the modal noise produced by the few-modes propagation within SSMF for the wavelength of 850 nm. In particular, the mutual interference of the LP_{01} and LP_{11} modes under temperature stress produces specific fluctuating behaviors of the amplitudes of DC and RF components of the detected current. This fact can be usefully exploited to fit the chirp parameters. Indeed, letting the fiber undergo linear temperature variation, the fluctuations feature a sinusoidal behavior with specific characteristics of amplitude and phase, which depend also on frequency chirping. Measuring the phase difference between the amplitude fluctuations of the RF component and the ones of the DC component of the detected current it is possible to directly measure the chirp parameters. The optical system considered (see Fig.1) is composed by a single mode, single polarization, 850 nm VCSEL, operating under RF direct modulation, followed by an optical isolator and by a strand of standard G.652 fiber with length L_{G652}. The G.652 fiber is followed in turn by a short span (length $L_{5\,\mu m}$) of customized fiber with 5 micron diameter ($\text{SMF}_{5\mu m}$), which is truly single-mode at 850 nm. As proved in [26], in this way the effect of modal noise is amplified. Indeed, contrary to application context, in the present case the presence of a strong modal noise is a desired feature of the system, since it allows to successfully apply the proposed measurement technique.

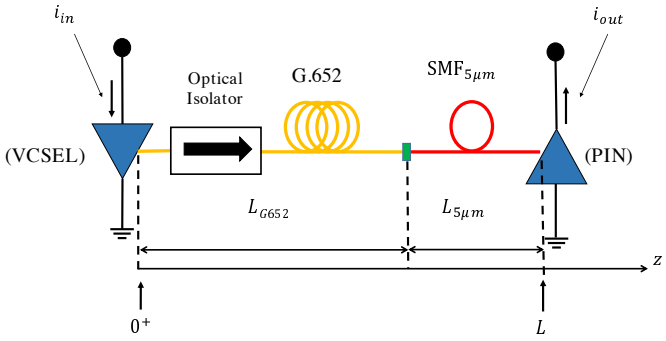

Fig. 1: Optical system considered. See text for details.

III. Theoretical Model

A. System considered and field emitted by the optical source

The current given in input to the VCSEL (see Fig.1) is $i_{in}(t) = I_{bias} + I_{RF,IN,M}\cos(\omega_{RF}t)$, where I_{bias} is the biasing current , while $I_{RF,IN,M}$ and $\omega_{RF} = 2\pi f_{RF}$ are respectively the amplitude and the angular frequency of the input RF current with f_{RF} indicating the RF frequency. The electrical field emitted by the optical source is given by the following relation:

$$\bar{E}(t) = E_0\bar{e}\sqrt{1 + m_I\cos(\omega_{RF}t)}e^{j[\omega_0 t + \Delta\theta(t)]} \quad (1)$$

where $\omega_0 = 2\pi f_0$ is the optical angular frequency with f_0 indicating the optical frequency, $m_I = I_{RF,IN,M}/(I_{bias} - I_{th})$ is the optical modulation index, with I_{th} indicating the threshold current of the VCSEL, and where $\Delta\theta(t)$ is the phase deviation due to the chirp phenomenon. The electrical field is directed along the unit vector $\bar{e}$ and its amplitude E_0 is given by:

$$E_0 = \sqrt{\eta_{TX}(I_{bias} - I_{th})} \quad (2)$$

where η_{TX} is the laser slope-efficiency. The total power related to the electrical field expressed by (1) can be written as follows:

$$P(t) = P_0[1 + m_I\cos(\omega_{RF}t)] \quad (3)$$

where $P_0 \propto |E_0|^2$. The chirp term $\Delta\theta(t)$ is given by the following general relation [27]:

$$\Delta\theta(t) = M(\omega_{RF})\sin(\omega_{RF}t + \psi(\omega_{RF})) \quad (4)$$

where $M(\omega_{RF})$ is the phase modulation index and $\psi(\omega_{RF})$ represents the phase-shift between the frequency modulation term (given by $\frac{1}{2\pi}\frac{d\Delta\theta(t)}{dt}$) and the amplitude modulation. These values can be related to the contribution of chirp due to *carrier* and *thermal* effects [28], where generally the latter dominate at very low frequencies (order of few MHz) while the carrier effects dominate at higher frequencies. Therefore the electrical field expressed in (1) is put in the following form:

$$\bar{E}(t) = E_0\bar{e}\sqrt{1+m_I\cos(\omega_{RF}t)}e^{j[\omega_0 t + M\sin(\omega_{RF}t+\psi)]} \quad (5)$$

The expression given by (5) will be used in the next sections to represent the ouput field of the laser.

B. Determination of the output photocurrent

In section $z = 0^+$ of the G.652 fiber (see again Fig.1) the guided electrical field is expressed as follows:

$$\bar{E}(t) = \sum_{m=1}^{N_{modes}} A_m\bar{e}_m\sqrt{1+m_I\cos(\omega_{RF}t)}\cdot \cdot e^{[j\omega_0 t + M\sin(\omega_{RF}t+\psi)]} \quad (6)$$

where m is the mode index, N_{modes} is the total number of guided modes, A_m and $\bar{e}_m$ are respectively the normalized amplitude and the normalized electrical field of the m-th mode. In the present case it is $N_{modes} = 2$, since only the LP_{01} and LP_{11} modes propagate at the operating wavelength $\lambda = 850\,nm$ within the G.652 fiber. A normalization with respect to the optical power coupled into the fiber is assumed, so that:

$$A_1^2 + A_2^2 = 1 \quad (7)$$

After the distance $z = L_{G652}$, immediately before propagating within the SMF$_{5\mu m}$ the expression of the electrical field becomes:

$$\bar{E}(t, L_{G652}) = \sum_{m=1}^{N_{modes}} A_m\bar{e}_m\cdot \cdot\sqrt{1+m_I\cos(\omega_{RF}(t-\tau_{m\,G652}))}\cdot \cdot e^{[j\omega_0 t - \beta_m(t)L_{G652} + M\sin(\omega_{RF}(t-\tau_{m\,G652})+\psi)]} \quad (8)$$

where β_m and $\tau_{m,\,G652}$ are respectively the propagation constant and the group delay of the m-th mode of the G.652 fiber. The quantity β_m varies in time because the G.652 fiber is supposed to be in an environment where the temperature is varying. Note that, rigorously speaking also the quantity $\tau_{m,\,G652}$ should be taken as varying in time. However the corresponding phase $\omega_{RF}\tau_{m,\,G652} = \omega_{RF}\hat{\tau}_{m,\,G652}L_{G652}$ where $\hat{\tau}_{m,\,G652}$ is the the group delay per unit length of the m-th mode of the G.652 fiber, changes with a speed which is slower with respect to $\beta_m(t)L_{G652}$ by a factor of $\omega_{RF}/\omega_0 \sim 10^{-5}$ and can therefore be regarded as constant [25], [29], [30].

The electrical field that comes out from the SMF$_{5\mu m}$ and goes to the photo-diode after a length $L = L_{G652} + L_{5\mu m}$ can be written as:

$$\bar{E}(t, L) = \left\{ \sum_{m=1}^{N_{modes}} A_m a_m\sqrt{1+m_I\cos(\omega_{RF}(t-\tau_m))} \; e^{[j\omega_0 t - \beta_m(t)L_{G652} + M\sin(\omega_{RF}(t-\tau_m)+\psi)]} \right\} \bar{e}_{5\mu m}e^{-j\beta_{5\mu m}L_{5\mu m}} \quad (9)$$

where $\bar{e}_{5\mu m}$ is the normalized electrical field of the fundamental mode which propagates inside the SMF$_{5\mu m}$ fiber ($LP_{01,5\mu m}$), while $\beta_{5\mu m}$ is its propagation constant. Moreover, it is $\tau_m = \tau_{m,G652} + \tau_{1,5\mu m}$, where $\tau_{1,5\mu m}$ is group delay of the $LP_{01,5\mu m}$ mode propagating in the SMF$_{5\mu m}$ fiber. The coupling coefficient a_m is computed exploiting the mode matching theory and is defined by the following integral over the cross-section S_{cross} between G652 fiber and SMF$_{5\mu m}$ fiber:

$$a_m = \iint_{S_{cross}} \bar{e}_m(x,y)\cdot\bar{e}^*_{5\mu m}(x,y)dxdy \quad (10)$$

Finally, the output current which comes out from the photodiode can be determined using the following equation:

$$i_{out}(t) = \int_{S_{PD}} |E(t,L)|^2 dS \quad (11)$$

where S_{PD} is the photodiode surface seen by the SMF$_{5\mu m}$ fiber.

Computing the integral in (11) we obtain:

$$\begin{aligned} &i_{out}(t) = \\ &\sum_{m=1}^{N_{modes}} A_m^2 a_m^2\,(1+m_I\cos(2\pi f_{RF}(t-\tau_m)) \\ &+ 2A_1a_1A_2a_2 \\ &\cdot[1+m_I\cos(2\pi f_{RF}\Delta\tau_{12})\cos(2\pi f_{RF}(t-\bar{\tau}_{12})] \\ &\cdot\Big[\cos(\Delta\beta_{12}(t))\cos(x_{12}\cos(2\pi f_{RF}(t-\bar{\tau}_{12})+\psi)) \\ &+ \sin(\Delta\beta_{12}(t))\sin(x_{12}\cos(2\pi f_{RF}(t-\bar{\tau}_{12})+\psi))\Big] \end{aligned} \quad (12)$$

where the following coefficients are defined:

$$x_{12} = 2M\sin(2\pi f_{RF}\Delta\tau_{12}) \quad (13)$$

$$\Delta\beta_{12}(t) = [\beta_1(t) - \beta_2(t)]L_{G652} \quad (14)$$

$$\bar{\tau}_{12} = \frac{\tau_1+\tau_2}{2} \quad (15)$$

$$\Delta\tau_{12} = \frac{\tau_1-\tau_2}{2} = \frac{\tau_{1,G652}-\tau_{2,G652}}{2} \quad (16)$$

The temperature variation mentioned above is assumed to be linear with time, and for this reason the quantity β_m ($m = 1, 2$) is assumed to vary linearly with time as well. It is then $\beta_m = \beta_{m,0} + \dot{\beta}_m t$ with $\dot{\beta}_m = \frac{d\beta_m}{dt}$, and $\Delta\beta_{12}(t) = \Delta\beta_{12,0} + \Delta\left(\dot{\beta}_{12}\right)t$ with $\Delta\beta_{12,0} = \beta_{1,0} - \beta_{2,0}$ and $\Delta\left(\dot{\beta}_{12}\right) = \dot{\beta}_1 - \dot{\beta}_2$. In the following to fix ideas it will be assumed $\Delta\left(\dot{\beta}_{12}\right) > 0$ without loss of generality of the theoretical model developed.

Equation (12) is composed of DC and RF components, which will be denoted as i_{DC} and i_{RF}. They can be written as:

$$i_{DC}(t) = I_{DC,0} + \Delta I_{DC}(t) \tag{17}$$

$$\begin{aligned} i_{RF}(t) &= \Re\left\{[I_{RF,\Re}(t) - jI_{RF,\Im}(t)]\, e^{j\omega_{RF}t}\right\} = \\ &= [I_{RF,\Re,0} + \Delta I_{RF,\Re}(t)]\cos(\omega_{RF}t) + \\ &+ [I_{RF,\Im,0} + \Delta I_{RF,\Im}(t)]\sin(\omega_{RF}t) \end{aligned} \tag{18}$$

where the notation $\Re\{(\cdot)\}$ means that the real part of $(\cdot)$ is taken. In Eq. (17) and (18) $I_{DC,0}, I_{RF,\Re,0}, I_{RF,\Im,0}$ are the mean values of the envelopes of DC component, real ($I_{RF,\Re}$) and imaginary ($I_{RF,\Im}$) RF components given by the following expressions:

$$I_{DC,0} = A_1^2 a_1^2 + A_2^2 a_2^2 \tag{19}$$

$$I_{RF,\Re,0} = m_I[A_1^2 a_1^2 \cos(\omega_{RF}\tau_1) + A_2^2 a_2^2 \cos(\omega_{RF}\tau_2)] \tag{20}$$

$$I_{RF,\Im,0} = m_I[A_1^2 a_1^2 \sin(\omega_{RF}\tau_1) + A_2^2 a_2^2 \sin(\omega_{RF}\tau_2)] \tag{21}$$

while $\Delta I_{DC}, \Delta I_{RF,\Re}, \Delta I_{RF,\Im}$ are the corresponding fluctuating terms of the envelopes which depend directly on the time variation of $\Delta\beta_{12}(t)$, and can be expanded as follows:

$$\Delta I_{DC}(t) = 2A_1 a_1 A_2 a_2 J_0(x_{12})\cos(\Delta\beta_{12}(t)) \tag{22}$$

$$\begin{aligned} &\Delta I_{RF,\Re}(t) = 2A_1 a_1 A_2 a_2 \cdot \\ &\cdot [m_I \cos(\omega_{RF}\Delta\tau_{12}) J_0(x_{12}) \cos(\omega_{RF}\bar{\tau}_{12}) \cos(\Delta\beta_{12}(t)) + \\ &+ 2J_1(x_{12}) \cos(\omega_{RF}\bar{\tau}_{12} + \psi)] \sin(\Delta\beta_{12}(t)) \end{aligned} \tag{23}$$

$$\begin{aligned} &\Delta I_{RF,\Im}(t) = 2A_1 a_1 A_2 a_2 \cdot \\ &\cdot [m_I \cos(\omega_{RF}\Delta\tau_{12}) J_0(x_{12}) \sin(\omega_{RF}\bar{\tau}_{12}) \cos(\Delta\beta_{12}(t)) + \\ &+ 2J_1(x_{12}) \sin(\omega_{RF}\bar{\tau}_{12} + \psi)] \sin(\Delta\beta_{12}(t)) \end{aligned} \tag{24}$$

C. Determination of the chirp parameters from the phase shifts between DC and RF components

Equations (22)-(24) show that while in the case of $\Delta I_{DC}(t)$ the time dependence is only given by a term proportional to $\cos(\Delta\beta_{12}(t))$, in the case of $\Delta I_{RF,\Re}(t)$ and $\Delta I_{RF,\Im}(t)$ it is given by two terms which are respectively proportional $\cos(\Delta\beta_{12}(t))$ and $\sin(\Delta\beta_{12}(t))$. This determines the presence of phase shifts of both $\Delta I_{RF,\Re}(t)$ and $\Delta I_{RF,\Im}(t)$ with respect to $\Delta I_{DC}(t)$. For a given value of ω_{RF}, their expressions are respectively given by:

$$\Delta\phi_{\Re,DC}(\omega_{RF}) = \tan^{-1}\left[\mathcal{U}(\omega_{RF}, M)\cdot\mathcal{V}_{\mathcal{C}}(\omega_{RF},\psi)\right] \tag{25}$$

$$\Delta\phi_{\Im,DC}(\omega_{RF}) = \tan^{-1}\left[\mathcal{U}(\omega_{RF}, M)\cdot\mathcal{V}_{\mathcal{S}}(\omega_{RF},\psi)\right] \tag{26}$$

where:

$$\mathcal{U}(\omega_{RF}, M) = \frac{2J_1(x_{12})}{m_I\cos(\omega_{RF}\Delta\tau_{12})J_0(x_{12})} \tag{27}$$

$$\mathcal{V}_{\mathcal{C}}(\omega_{RF},\psi) = \cos(\omega_{RF}\bar{\tau}_{12}+\psi)/\cos(\omega_{RF}\bar{\tau}_{12}) \tag{28}$$

$$\mathcal{V}_{\mathcal{S}}(\omega_{RF},\psi) = \sin(\omega_{RF}\bar{\tau}_{12}+\psi)/\sin(\omega_{RF}\bar{\tau}_{12}) \tag{29}$$

The method which is here proposed consists in determining experimentally $\Delta\phi_{\Re,DC}(\omega_{RF})$, $\Delta\phi_{\Im,DC}(\omega_{RF})$, and subsequently extracting the values of $M(\omega_{RF})$, $\psi(\omega_{RF})$ from the inversion of respectively Eq. (25) and Eq. (26).

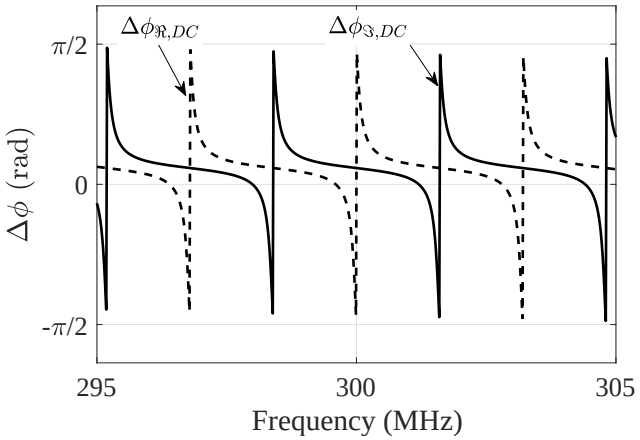

Fig. 2: Example of theoretical behaviors of $\Delta\phi_{\Re,DC} = \tan^{-1}\left[\mathcal{U}\cdot\mathcal{V}_{\mathcal{C}}\right]$ and $\Delta\phi_{\Im,DC} = \tan^{-1}\left[\mathcal{U}\cdot\mathcal{V}_{\mathcal{S}}\right]$ for different values of M, ψ. Note that the functions exhibit fast variations with respect to f_{RF} even in the short frequency interval considered. See text for details.

This extraction procedure for a given ω_{RF} not only requires the measurement of $\Delta\phi_{\Re,DC}$, $\Delta\phi_{\Im,DC}$ at ω_{RF}, but also in the vicinity of that angular frequency.
Indeed, as will be shown with greater detail in Appendix I, the functions $\mathcal{V}_{\mathcal{C}}(\omega_{RF},\psi)$, $\mathcal{V}_{\mathcal{S}}(\omega_{RF},\psi)$ exhibit for varying ω_{RF} tangentoid−like behaviors with a periodicity which is of a few MHz when the value of the length L of the fiber connection is of the order of a few tens of meters. This determines in turn a fast variation of the second sides of Equations (25) and (26) even within relatively small frequency intervals in the vicinity of a given value ω_{RF}. Fig. 2 shows examples of theoretical behaviors of these functions for different values of M and ψ in a short interval centered in $f_{RF} = 300\,MHz$, utilizing typical values for the parameters involved.

As a consequence of this, it is necessary to have at disposal a high number of measured values of $\Delta\phi_{\Re,DC}$ and $\Delta\phi_{\Im,DC}$ in the vicinity of ω_{RF} in order to perform the extraction operation with satisfactory accuracy. The extraction procedure can be applied independently either determining experimentally the values of $\Delta\phi_{\Re,DC}$ at various frequencies centered in f_{RF} and then inverting Eq. (25), or determining similarly the values of $\Delta\phi_{\Im,DC}$ and then inverting Eq. (26). Both procedures lead to obtain the same values of $M(\omega_{RF})$, $\psi(\omega_{RF})$. In the remainder, the focus will be maintained to the former procedure, namely the one which exploits the inversion of Eq. (25).
In Appendix I further details on the procedure for computing M and ψ are given. Indeed, the procedure implied a particular post-processing of Equation (25) which allows to find separately the two parameters.

IV. Experimental Application of the Method

A. Measurement setup

The experimental setup is shown in Figure 3. A Vectorial Network Analyzer (VNA) is used to generate and receive radio frequency sinusoidal signals. In particular, port 1 is used to

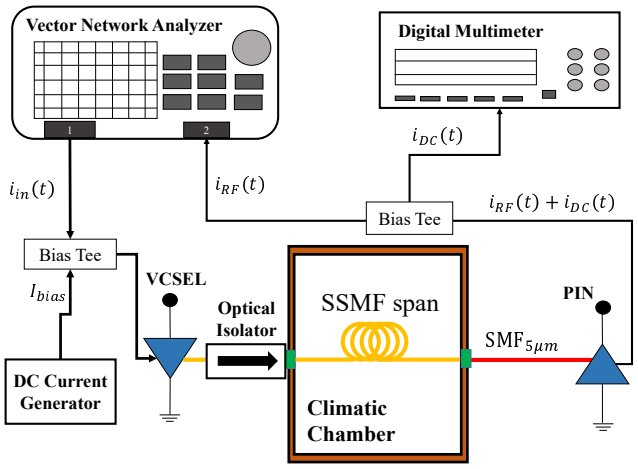

Fig. 3: Experimental setup for the measurement of VCSEL chirp. See text for details.

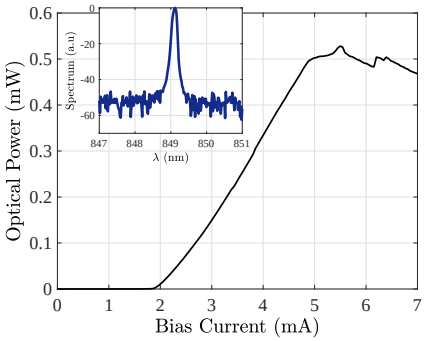

Fig. 4: LIV curve and optical spectrum (inset) for the SM VCSEL considered.

inject RF power into the VCSEL, while port 2 is used to receive the RF signal which comes out from the photodiode. Both VCSEL and PIN photodiode are connected to a bias tee which allows respectively to inject in transmission and measure in reception the DC component of the current. The L-I curve and the optical spectrum of the VCSEL are shown in Figure 4. The laser is connected to 30 meters of G.652 fiber placed into a controlled climatic chamber. Temperature variations are forced within the chamber and are subsequently monitored by an external data acquisition block. After the G.652 fiber, a short span (3 meters) of $SMF_{5\mu m}$ (Thorlabs 780HP) is connected to a photodiode. The latter fiber is placed to force important modal noise fluctuations as reported in [26]. Note indeed that the effect produced by modal noise, which is typically regarded as detrimental, is exploited advantageously in this case and is therefore amplified to better measure the phase shift between the fluctuating components of DC and RF output currents.

As specified in the previous Section, in order to perform correctly the extraction of the parameters $M(\omega_{RF})$, $\psi(\omega_{RF})$ for a given frequency $f_{RF} = \omega_{RF}/(2\pi)$, the measured values of $\Delta\phi_{\Re,DC}$ (or $\Delta\phi_{\Im,DC}$) should be available for a high number of frequencies in the vicinity of ω_{RF}. For this reason the measurement is performed in correspondence to 1001 equally spaced frequencies located in a small interval centered in f_{RF}. The width of such interval has been chosen as $10\,MHz$.

For each one of such frequencies, data from VNA and acquisition block are taken with a period of one second, which is appropriate in view the subsequent processing of the received signal, which is based on its Discrete Fourier Transform (DFT). Indeed, with the temperature variations imposed in the experiments, the periods of the fluctuating behaviors of $\Delta I_{DC}(t)$ and $\Delta I_{RF,\Re}(t)$, (and also of $\Delta I_{RF,\Im}(t)$) do not fall in any case below values of tens of seconds.

The frequencies considered for determining $M(\omega_{RF})$ and $\psi(\omega_{RF})$ ranged from $100\,MHz$ to $1.5\,GHz$ with intervals of $50\,MHz$. The value of the OMI has always been kept lower than 10%.

B. Experimental results

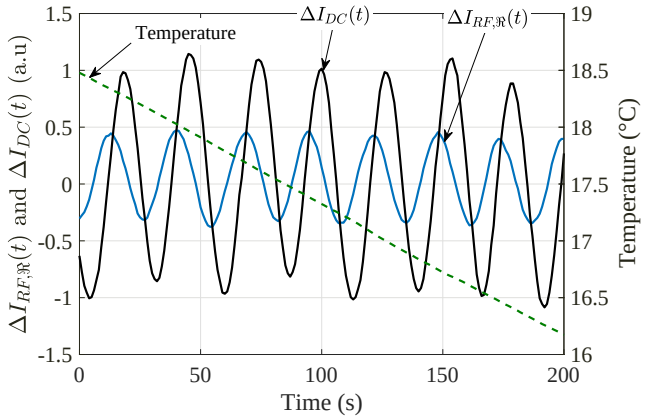

Fig. 5: Typical measurement in the time domain of $\Delta I_{DC}(t)$ and $\Delta I_{RF,\Re}(t)$. The value of the modulating frequency is $f_{RF} = 300\,MHz$. The phase shift between the two fluctuating behaviors is clearly visble. In this case it is $\Delta\phi_{\Re,DC} \simeq -0.075$ rad.

As mentioned above, for each one of the RF frequencies considered, after having performed the time measurements of $\Delta I_{DC}(t)$ and $\Delta I_{RF,\Re}(t)$ (see Fig. 5), the DFT is applied to the time waveforms to extrapolate the phase difference $\Delta\hat{\phi}_{\Re,DC}$. Figure 6 shows typical measured values of $\Delta\hat{\phi}_{\Re,DC}$ for different centered frequencies f_{RF}.

As will be shown in the Appendix, starting from the experimentally measured values of $\Delta\hat{\phi}_{\Re,DC}$ and exploiting the relationship given by (25) it is possible to finally determine the values of $M(\omega_{RF})$ and $\psi(\omega_{RF})$.

Note that to estimate properly the value of M and ψ the group delay difference per unit length $\Delta\hat{\tau}_{12}$ has to be separately measured . This can be done considering the frequency response of an optical link where the VCSEL is followed by a strand of G652 fiber with length L_{test} ending in a photodetector (i.e. the system depicted in Fig.1 where the $SMF_{5\mu m}$ is removed).

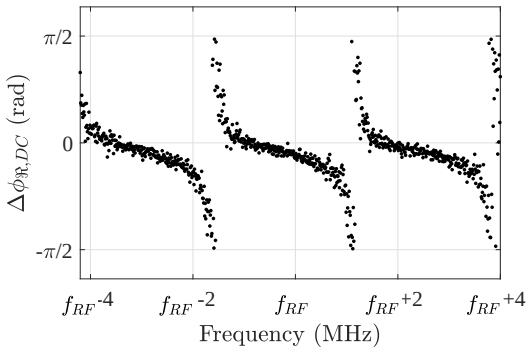

(a) $f_{RF} = 300\,MHz$

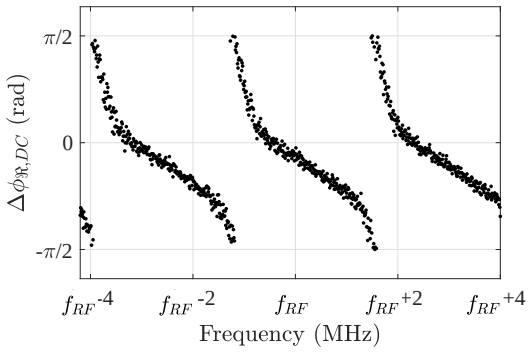

(b) $f_{RF} = 600\,MHz$

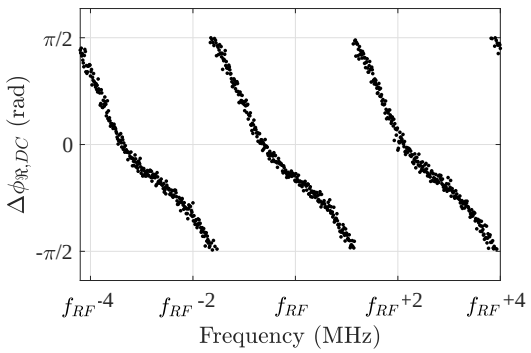

(c) $f_{RF} = 1000\,MHz$

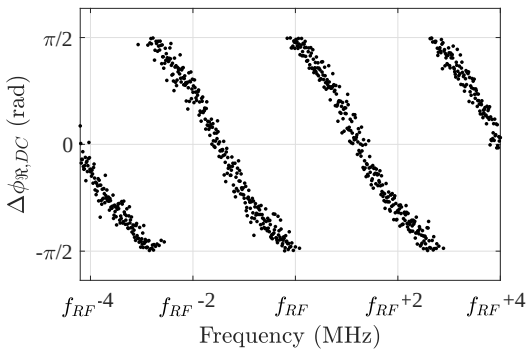

(d) $f_{RF} = 1400\,MHz$

Fig. 6: Example of four difference measurments of $\Delta\phi_{\Re,DC}$ for different center frequencies f_{RF}.

Considering the frequency f_{min} which corresponds to the first minimum of the response it is obtained [13]:

$$\Delta\hat{\tau}_{12} = \frac{1}{2f_{\min}L_{test}} \tag{30}$$

In the present case it was $L_{test} = 300m$ and it was found $\Delta\hat{\tau}_{12} = 2.38\,ps/m$. The values obtained of M and ψ through the application of the proposed method are shown in Figure 7. Note that M is shown performing a normalization with respect to the optical modulation index m_I, which shows directly the FM/AM relation.

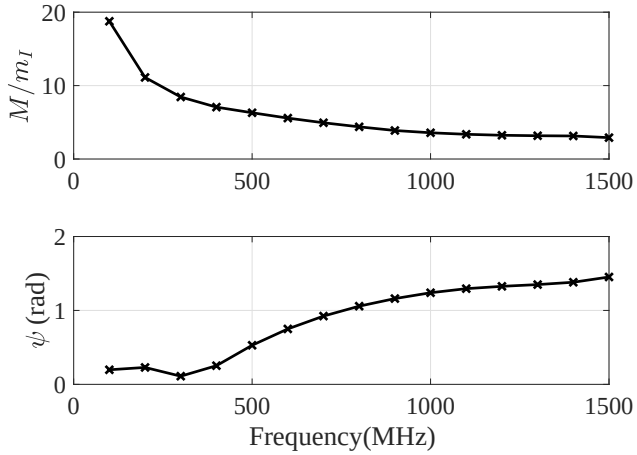

Fig. 7: Results obtained from the implementation of the method proposed.

C. Validation of the method

The chirp characterization of the same laser source has been performed also employing the procedure described in [17]. As mentioned in the Introduction, the application of this method requires that the system operates in single−mode regime, and is consequently suited for characterizing laser sources operating in the second and third optical windows. To realize this technique a number of components exhibiting a truly single mode behavior at $850\,nm$ have been utilized, including a strand $100\,m$ long of $\text{SMF}_{5\mu m}$ fiber, which may not be typically present in an optics laboratory. The purpose of performing the measurement also with this technique was however to validate the method proposed. The comparison of the two methods are shown in Figure 8 for two different values of bias current. An average relative difference among the two methods has been found to be around 10% with a standard deviation of 5.5% which are quantities considered acceptable. To have a further validation, the method has been also applied fixing $f_{RF} = 800\,MHz$ for different values of biasing current I_{bias} (see Figure 9). An average difference among the two methods has been found to be about 12% with a standard deviation of 6%. Note that in this case the laser presents a minimum of M/m_I (therefore of M) for $I_{bias} = 4\,mA$, which can be exploited to improve the quality of transmission. Moreove, this type of behavior is also in according to what has been observed for other semiconductor lasers [31].

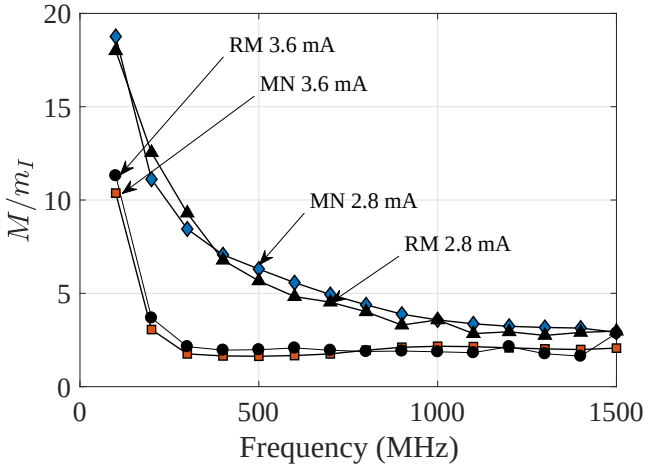

Fig. 8: Comparison between the proposed technique based on Modal Noise (MN) and the Reference Method (RM) proposed in [17]. The comparison is shwon for two different level of biasing.

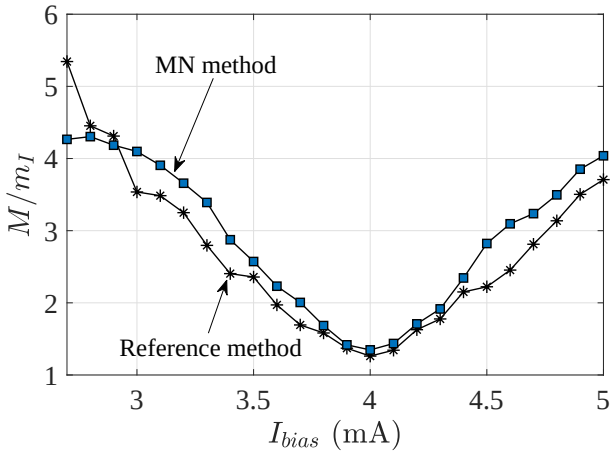

Fig. 9: Application of the proposed (MN) and reference method for $f_{RF} = 800\,MHz$ for different values of I_{bias}.

V. Conclusion

In this paper an innovative technique to characterize the chirp behavior of a single mode laser operating at 850 nm (e. g. low-cost, low-consumption VCSELs) has been proposed. Through this technique, which takes advantage of the two-modes propagation of the electromagnetic field at 850 nm within a G.652 fiber, it is possible to extrapolate the complete chirp characteristics of a single mode VCSEL by analyzing the fluctuations due to modal noise in both DC and RF components of the detected photocurrent. The method has been validated having a maximum relative difference of 12% compared to the delayed self-homodyne method taken as a reference. The technique requires low cost components and typical laboratory equipments and can then be directly applied whenever an accurate design of optical links operating in the first optical window has to be performed.

Acknowledgments

The authors thank Ing. Sebastiano Cucinotta for useful discussions about the mathematical framework of the presented method.

Appendix I

A. Evaluation of M and ψ from the phase differences between RF and DC fluctuating components of the photocurrent

The expression of $\Delta\phi_{\Re,DC}$ given by equation (25) depends in turn on the relations expressed by equations (27) and (28). The first one contains the information about M (through x_{12}, given by Eq. (13)), while the other one about ψ.
Note that in case the assumption $\psi \simeq 0$ could be taken, it would be $\mathcal{V}_{\mathcal{C}} \simeq \mathcal{V}_{\mathcal{S}} \simeq 1$ and both Eq. (25) and Eq. (26) would become

$$\Delta\phi_{\Re,DC} \simeq \Delta\phi_{\Im,DC} \simeq \tan^{-1}\left[\mathcal{U}(\omega_{RF}, M)\right] \qquad (31)$$

This was the case reported in [25] in which the adiabatic frequency chirp of DFB lasers operating in the second and third optical windows could be determined through the interference resulting from splitting and subsequent recombining of the LP_{01} mode propagating in G652 fiber strands. However, the present case is more general, and this assumption cannot be applied. The value of M will then have to be determined also for operating conditions where the value of ψ cannot be neglected, i.e. both M and ψ must be extracted from Eq. (25) and Eq. (26).

To identify the contribution of each of these two variables on Eq. (25) the function $\mathcal{V}_{\mathcal{C}}(\omega_{RF}, \psi)$ is initially considered, It can indeed be observed that such function is periodical in ω_{RF} (or f_{RF}) with period given by $\Omega = \pi/\bar{\tau}_{12}$ (or $F = 1/(2\bar{\tau}_{12})$). Since it is $\bar{\tau}_{12} \simeq 0.5 \cdot 10^{-9} \cdot L$, with L in the order of tens of meters, the value of F is of the order of a few MHz. Within this interval, $\mathcal{V}_{\mathcal{C}}(\omega_{RF}, \psi)$ encompasses all the values in the interval $]-\infty, \infty[$. A reasonable approximation that can be taken at this point is that in the range of frequencies Δf_{RF} given by a very few periods F (or, equivalently, in the range of angular frequencies $\Delta\omega_{RF}$ given by a very few periods Ω) the variations of M and ψ with respect to frequency are much slower than the ones of $\mathcal{V}_{\mathcal{C}}(\omega_{RF}, \psi)$.

Indeed, considering a reference angular frequency $\overline{\omega}_{RF} \in 2\pi \cdot [100, 1500]\,MHz$, and typical operating conditions, for a generic $\omega_{RF} \in \Delta\overline{\omega}_{RF} = [\overline{\omega}_{RF} - \Delta\omega_{RF}/2, \overline{\omega}_{RF} + \Delta\omega_{RF}/2]$ it is in line with the models generally assumed in literature [4], [32] to take:

$$\left|\frac{\partial M}{\partial \omega_{RF}}(\omega_{RF} - \overline{\omega}_{RF})\right| << |M(\overline{\omega}_{RF})| \qquad (32)$$

$$\left|\frac{\partial \psi}{\partial \omega_{RF}}(\omega_{RF} - \overline{\omega}_{RF})\right| << |\psi(\overline{\omega}_{RF})| \qquad (33)$$

This practically means that within the interval $\Delta\omega_{RF}$ centered in $\overline{\omega}_{RF}$ the values of M and ψ can be considered to be constant: $M|_{\omega_{RF} \in \Delta\overline{\omega}_{RF}} \simeq M(\overline{\omega}_{RF})$, $\psi|_{\omega_{RF} \in \Delta\overline{\omega}_{RF}} \simeq \psi(\overline{\omega}_{RF})$.

Remembering that it is $\Delta\tau_{12} \sim 10^{-12} \cdot L$, the same considerations can be applied to the function $\mathcal{U}$ given by Eq.

(27), which will be considered to be constant in the same interval: $\mathcal{U}|_{\omega_{RF}\in\Delta\overline{\omega}_{RF}} \simeq \mathcal{U}(\overline{\omega}_{RF}, M(\overline{\omega}_{RF}))$.

The considerations developed above simplify equation (25) and allow to operate in a single interval $\Delta\overline{\omega}_{RF}$ around the desired frequency $\overline{\omega}_{RF}$, in which equation (25) can be written as follows:

$$\begin{aligned}&\Delta\phi_{\Re,DC} = \\ &= \tan^{-1}\left(\mathcal{U}(\overline{\omega}_{RF}, M(\overline{\omega}_{RF})) \cdot \mathcal{V}_{\mathcal{C}}(\omega_{RF}, \psi(\overline{\omega}_{RF}))\right)\end{aligned} \tag{34}$$

To separate the contributions of M and ψ to $\Delta\phi_{\Re,DC}$, a procedure is utilized which requires two steps.

The first one consists in computing the absolute value of $\Delta\phi_{\Re,DC}$ and subsequently perform its average on the frequency values. Formally, the expression can be written as $< |\Delta\phi_{\Re,DC}| >$ in which $< \cdot >$ is the frequency mean operator. The operation of averaging allows to achieve the independence of the function on the periodicity in ω_{RF} of $\mathcal{V}_{\mathcal{C}}(\omega_{RF}, \psi(\overline{\omega}_{RF}))$, while performing the absolute value allows to achieve its independence (or weak dependence) on the quantity ψ.

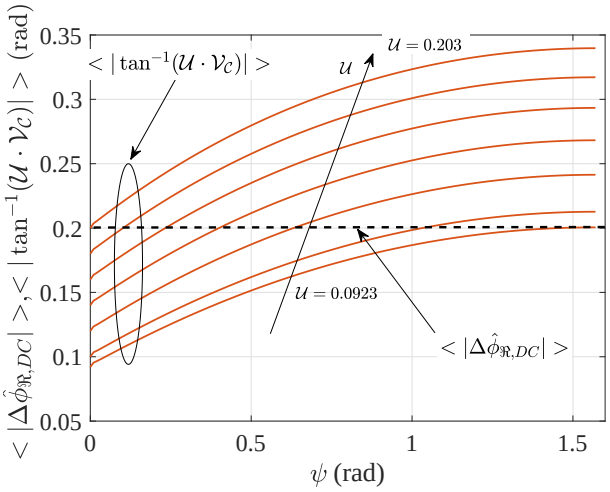

Fig. 10: Dependence of the function $< |\Delta\phi_{\Re,DC}| >$ on the variable ψ fixing different values of $\mathcal{U}$. The intersections of those curves with the measured value $< |\Delta\hat{\phi}_{\Re,DC}| >$ restrict the possible solution to a small interval of $\mathcal{U}$.

This point is further detailed in Figures 10 and 11. Note that in Figure 10 the intersections between the hypothetical measured value $< |\Delta\hat{\phi}_{\Re,DC}| >$ and the functions $< |\tan^{-1}(\mathcal{U}\cdot\mathcal{V}_{\mathcal{C}})| >$ give a restricted interval of possible solutions of $\mathcal{U}$, which constitutes a useful first step for the resolution of the problem. In Figure 11 instead, the intersections between $< \Delta\hat{\phi}_{\Re,DC} >$ and $< \tan^{-1}(\mathcal{U}\cdot\mathcal{V}_{\mathcal{C}}) >$ produce a larger range of possible values of $\mathcal{U}$ and ψ which makes the problem indeterminate.

Figure 12 shows this first step of the procedure in which the following relation is solved:

$$\begin{aligned}&< |\Delta\hat{\phi}_{\Re,DC}| >= \\ &=< |\tan^{-1}\left(\mathcal{U}(\overline{\omega}_{RF}, M(\overline{\omega}_{RF})) \cdot \mathcal{V}_{\mathcal{C}}(\omega_{RF}, \psi(\overline{\omega}_{RF}))\right)| >\end{aligned} \tag{35}$$

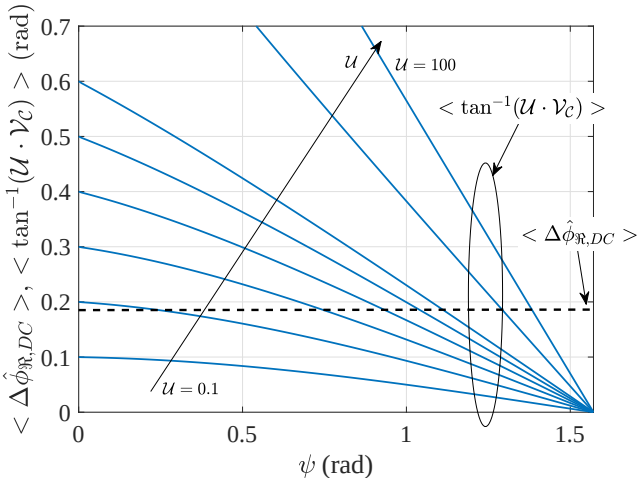

Fig. 11: Dependence of the function $< \Delta\phi_{\Re,DC} >$ on the variable ψ fixing different values of $\mathcal{U}$. In this case the range of possible values of $\mathcal{U}$ is larger, making the resolution of the problem difficult.

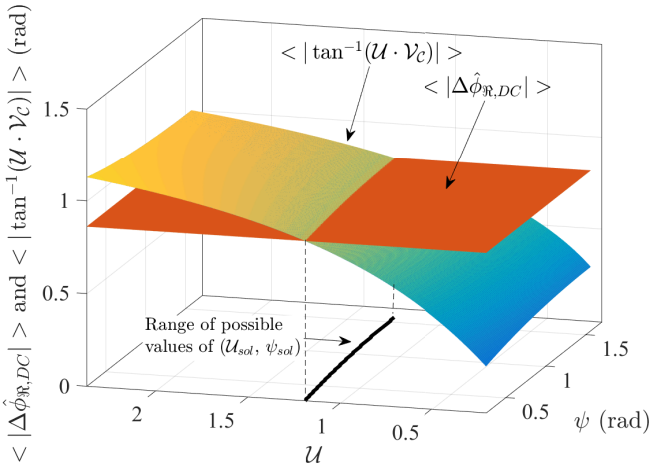

Fig. 12: 3D plot of the function $< |\Delta\phi_{\Re,DC}| >$ and of the plane $< |\Delta\hat{\phi}_{\Re,DC}| >$. The intersection produces possible couples of solution $(\mathcal{U}_{sol}, \psi_{sol})$.

in which $\Delta\hat{\phi}_{\Re,DC}$ represents the measured phase-shift among RF real part and DC component of the output current. Eq. (35) allows to find a first set of possible solutions $(\mathcal{U}_{sol}, \psi_{sol})$ where $\mathcal{U}_{sol}$ belongs to a restricted region in the sorrounding of $\tan\left(< |\Delta\hat{\phi}_{\Re,DC}| >\right)$, while $\psi_{sol} \in [0, \pi/2]$. It can be appreciated in Figure 12 that the application of the operator $< |\cdot| >$ makes the possible values of $\mathcal{U}_{sol}$ to fall into to a quite restricted region.

The second and final step of the procedure consists in considering the solutions $(\mathcal{U}_{sol}, \psi_{sol})$ determined at the first step and determine among them the one which solves the equation:

$$\begin{aligned}&< \Delta\hat{\phi}_{\Re,DC} >= \\ &=< \tan^{-1}\left(\overline{\mathcal{U}}_{sol}(\overline{\omega}_{RF}, M(\overline{\omega}_{RF})) \cdot \mathcal{V}_{\mathcal{C}}(\omega_{RF}, \overline{\psi}_{sol}(\overline{\omega}_{RF}))\right) >\end{aligned} \tag{36}$$

which coincides with Equation (35) save for the absence of computation of the absolute value. This operation allows to identify the the exact solution $(\overline{\mathcal{U}}_{sol}, \overline{\psi}_{sol})$ of the problem.

After having solved Equation (36), the extrapolation of M from $\overline{\mathcal{U}}_{sol}(\overline{\omega}_{RF}, M(\overline{\omega}_{RF}))$ can be directly performed from Equation (27).

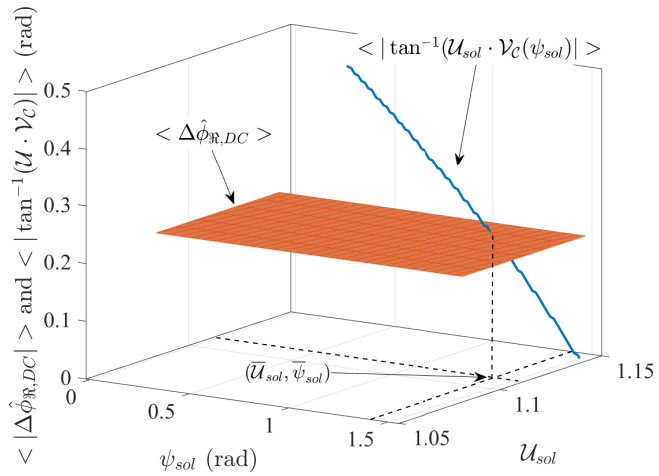

Fig. 13: 3D plot of the function $< \Delta\phi_{\Re,DC} >$ computed in the values founded in the first step $(\mathcal{U}_{sol}, \psi_{sol})$. The intersection with the plane corresponding to $< \Delta\hat{\phi}_{\Re,DC} >$ gives the final solution.

REFERENCES

[1] M. Feng, C. H. Wu, and N. Holonyak, "Oxide-confined vcsels for high-speed optical interconnects," *IEEE J. Quantum Electron.*, vol. 54, no. 3, pp. 1–15, June 2018.

[2] J. P. Turkiewicz, J. R. Kropp, N. N. Ledentsov, V. A. Shchukin, and G. Schfer, "High speed optical data transmission with compact 850 nm to-can assemblies," *IEEE J. Quantum Electron.*, vol. 50, no. 4, pp. 281–286, April 2014.

[3] J. Guillory *et al.*, "Comparison between two 60GHz multipoint RoF architectures for the Home Area Network," in *17th European Conf. on Networks and Optical Commun. (NOC)*, Vilanova i la Geltru, Spain, June 2012, pp. 1–5.

[4] G. P. Agrawal and N. K. Dutta, *Semiconductor Lasers*. Springer US, 1993.

[5] G. Agrawal, "Power spectrum of directly modulated single-mode semiconductor lasers: Chirp-induced fine structure," *IEEE J. Quantum Electron.*, vol. 21, no. 6, pp. 680–686, Jun 1985.

[6] S. Kobayashi, Y. Yamamoto, M. Ito, and T. Kimura, "Direct frequency modulation in algaas semiconductor lasers," *IEEE J. Quantum Electron.*, vol. 18, no. 4, pp. 582–595, Apr 1982.

[7] G. Meslener, "Chromatic dispersion induced distortion of modulated monochromatic light employing direct detection," *IEEE J. Quantum Electron.*, vol. 20, pp. 1208–1216, 1984.

[8] D. Visani, G. Tartarini, L. Tarlazzi, and P. Faccin, "Transmission of UMTS and WIMAX Signals Over Cost-Effective Radio Over Fiber Systems," *IEEE Trans. Microw. Wireless Compon. Lett.*, vol. 19, no. 12, pp. 831–833, Dec 2009.

[9] M. Ahmed, A. Bakry, and S. W. Z. Mahmoud, "Influence of Chirp of High-Speed Laser Diodes and Fiber Dispersion on Performance of Non-Amplified 40-Gbps Optical Fiber Links," *International J. Math., Computational, Physical, Elect. and Comput. Eng.*, vol. 9, no. 1, pp. 12–16, 2015.

[10] D. Visani, G. Tartarini, M. N. Petersen, L. Tarlazzi, and P. Faccin, "Link design rules for cost-effective short-range radio over multimode fiber systems," *IEEE Trans. Microw. Theory Tech.*, vol. 58, no. 11, pp. 3144–3153, Nov 2010.

[11] A. Koonen, "Bit-error-rate degradation in a multimode fiber optic transmission link due to modal noise," *IEEE J. Select. Areas in Commun.*, vol. 4, no. 9, pp. 1515–1522, Dec 1986.

[12] G. Alcaro, D. Visani, L. Tarlazzi, P. Faccin, and G. Tartarini, "Distortion mechanisms originating from modal noise in radio over multimode fiber links," *IEEE Trans. Microw. Theory Tech.*, vol. 60, no. 1, pp. 185–194, Jan 2012.

[13] J. Nanni *et al.*, "Modal noise in 850nm VCSEL-based radio over fiber systems for manifold applications," in *Fotonica AEIT Italian Conf. Photonics Technologies*, Turin, Italy, May 2015, pp. 1–4.

[14] I. Papakonstantinou, S. Papadopoulos, C. Soos, J. Troska, F. Vasey, and P. Vichoudis, "Modal Dispersion Mitigation in Standard Single-Mode Fibers at 850 nm With Fiber Mode Filters," *IEEE Photonics Technol. Lett.*, vol. 22, no. 20, pp. 1476–1478, Oct 2010.

[15] R. Beresford, "ASKAP photonic requirements," in *Intern. Topical Meeting on Microwave Photonics/Asia-Pacific Microwave Photonics Conf.*, Sept 2008, pp. 62–65.

[16] D. M. Baney and W. V. Sorin, "Measurement of a modulated DFB laser spectrum using gated delayed self-homodyne technique," *Electron. Lett.*, vol. 24, no. 11, pp. 669–670, May 1988.

[17] U. Kruger and K. Kruger, "Simultaneous measurement of the linewidth, linewidth enhancement factor α and FM and AM response of a semiconductor laser," *J. Lightw. Technol.*, vol. 13, no. 4, pp. 592–597, Apr 1995.

[18] W. V. Sorin, K. W. Chang, G. A. Conrad, and P. R. Herndday, "Frequency domain analysis of an optical fm discriminator," *J. Lightw. Technol.*, vol. 10, no. 6, pp. 787–793, Jun 1992.

[19] H. Halbritter, R. Shau, F. Riemenschneider, B. Kogel, M. Ortsiefer, J. Rosskopf, G. Bohm, M. Maute, M. C. Amann, and P. Meissner, "Chirp and linewidth enhancement factor of 1.55 μm VCSEL with buried tunnel junction," *Electron. Lett.*, vol. 40, no. 20, pp. 1266–1268, Sept 2004.

[20] H. Halbritter, F. Riemenschneider, J. Jacquet, J. G. Provost, C. Symonds, I. Sagnes, and P. Meissner, "Chirp and linewidth enhancement factor of tunable, optically-pumped long wavelength VCSEL," *Electron. Lett.*, vol. 40, no. 4, pp. 242–244, Feb 2004.

[21] C. Harder, K. Vahala, and A. Yariv, "Measurement of the linewidth enhancement factor alpha of semiconductor lasers," *Appl. Phys. Lett.*, no. 4, pp. 328–330, 1983.

[22] A. J. Faulkner and J. G. B. de Vaate, "Ska low frequency aperture array," in *IEEE Int. Symp. Antennas and Propagation USNC/URSI National Radio Science Meeting*, July 2015, pp. 1368–1369.

[23] J. Nanni, J. L. Polleux, C. Algani, S. Rusticelli, F. Perini, and G. Tartarini, "VCSEL-based Radio-over-G652 Fiber System for short/medium range MFH solutions," *J. Lightw. Technol.*, vol. PP, no. 99, pp. 1–1, 2018.

[24] J. Nanni, F. Pizzuti, G. Tartarini, J. L. Polleux, and C. Algani, "VCSEL-SSMF-based Radio-over-Fiber link for low cost and low consumption wireless dense networks," in *Proc. Int. Topical Meeting Microw. Photonics (MWP)*, Beijing, China, Oct 2017, pp. 1–4.

[25] J. Nanni, M. Barbiroli, F. Fuschini, D. Masotti, J. Polleux, C. Algani, and G. Tartarini, "Chirp evaluation of semiconductor DFB lasers through a simple Interferometry-Based (IB) technique," *Appl. Opt.*, vol. 55, no. 28, pp. 7788–7795, Oct 2016.

[26] J. Nanni, S. Rusticelli, C. Viana, J. L. Polleux, C. Algani, F. Perini, and G. Tartarini, "Modal Noise Mitigation in 850-nm VCSEL-Based Transmission Systems Over Single-Mode Fiber," *IEEE Trans. Microw. Theory Techn.*, vol. 64, no. 10, pp. 3342–3350, Oct 2016.

[27] E. Peral, W. K. Marshall, and A. Yariv, "Precise measurement of semiconductor laser chirp using effect of propagation in dispersive fiber and application to simulation of transmission through fiber gratings," *J. Lightw. Technol.*, vol. 16, no. 10, pp. 1874–1880, Oct 1998.

[28] M. L. M. Larry A. Coldren, Scott W. Corzine, *Diode Lasers and Photonic Integrated Circuits*, 2nd ed., Wiley, Ed., April 2012.

[29] M. Bousonville and J. Rausch, "Velocity of signal delay chenges in fibre optic cable," in *Proc. of DIPAC09*, Basel, Switzerland, May 2009, pp. 248–250.

[30] L. Hoffmann, M. S. Müller, S. Krämer, M. Giebel, G. Schwotzer, and T. Wieduwilt, "Applications of fibre optic temperature measurement," in *Proc. Estonian Acad. Sci. Eng.*, 2007, pp. 363–378.

[31] L. Olofsson and T. G. Brown, "Frequency dependence of the chirp factor in 1.55 μm distributed feedback semiconductor lasers," *IEEE Photonics Technol. Lett.*, vol. 4, no. 7, pp. 688–691, July 1992.

[32] T. Fordell and A. M. Lindberg, "Experiments on the linewidth-enhancement factor of a vertical-cavity surface-emitting laser," *IEEE J. Quantum Electron.*, vol. 43, no. 1, pp. 6–15, Jan 2007.